Supporting Information

Organic Semiconducting Polymer Nanoparticles for Photoacoustic Labelling and Tracking of Stem Cells in the Second Near-Infrared Window

Chao Yin,[†,||] *Guohua Wen,*[‡,||] *Chao Liu,*[‡,||] *Boguang Yang,*[†] *Sien Lin,*[¶,§,¤] *Jiawei Huang,*[&] *Pengchao Zhao,*[†] *Siu Hong Dexter Wong,*[†] *Kunyu Zhang,*[†] *Xiaoyu Chen,*[†] *Gang Li,*[¶, §,^] *Xiaohua Jiang,*[&] *Jianping Huang,*[¶] *Kanyi Pu,*[*,#] *Lidai Wang,*[*,‡,°] *and Liming Bian*[*,†,¤,+,•,Δ]

[†]Department of Biomedical Engineering, The Chinese University of Hong Kong, Shatin, New Territories, Hong Kong, China

[‡]Department of Biomedical Engineering, City University of Hong Kong, 83 Tat Chee Ave, Kowloon, Hong Kong, China

[¶]Department of Orthopaedics & Traumatology, Faculty of Medicine, The Chinese University of Hong Kong, Prince of Wales Hospital, Shatin, Hong Kong, China

[§]Stem Cells and Regenerative Medicine Laboratory, Lui Che Woo Institute of Innovative Medicine, Li Ka Shing Institute of Health Sciences, The Chinese University of Hong Kong, Prince of Wales Hospital, Shatin, Hong Kong, China

[¤]Translational Research Centre of Regenerative Medicine and 3D Printing Technologies of Guangzhou Medical University, The Third Affiliated Hospital of Guangzhou Medical University, Guangzhou, P.R. China

[&]School of Biomedical Sciences, Faculty of Medicine, The Chinese University of Hong Kong, Hong Kong, China

[^]The CUHK-ACC Space Medicine Centre on Health Maintenance of Musculoskeletal System, The Chinese University of Hong Kong Shenzhen Research Institute, Shenzhen 518172, China

[#]School of Chemical and Biomedical Engineering, Nanyang Technological University, 70 Nanyang Drive, 637457 Singapore

[°]City University of Hong Kong Shenzhen Research Institute, Yuexing Yi Dao, Nanshan District, Shenzhen, Guang Dong, 518057, China

[+]Shenzhen Research Institute, The Chinese University of Hong Kong, Shenzhen 518172, China

[•]China Orthopedic Regenerative Medicine Group (CORMed), Hangzhou, Zhejiang 310058, China

[Δ]Centre for Novel Biomaterials, Chinese University of Hong Kong

[*]Address correspondence to:

kypu@ntu.edu.sg

lidawang@cityu.edu.hk

lbian@cuhk.edu.hk

[‖]Both authors contributed equally to this work.

1. Supporting Figures

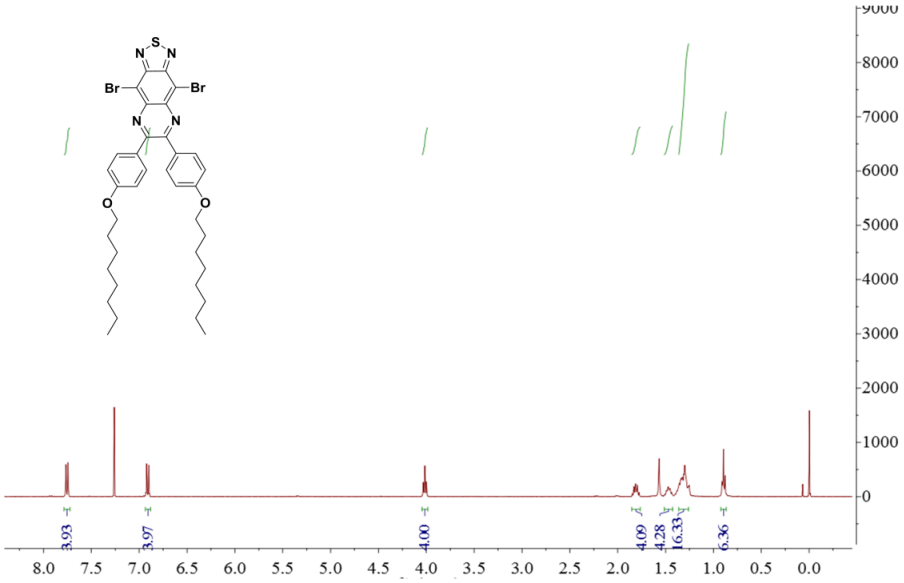

Supporting Figure S1. ^{1}H NMR of monomer 1 (M1). $CDCl_3$ was used as the solvent.

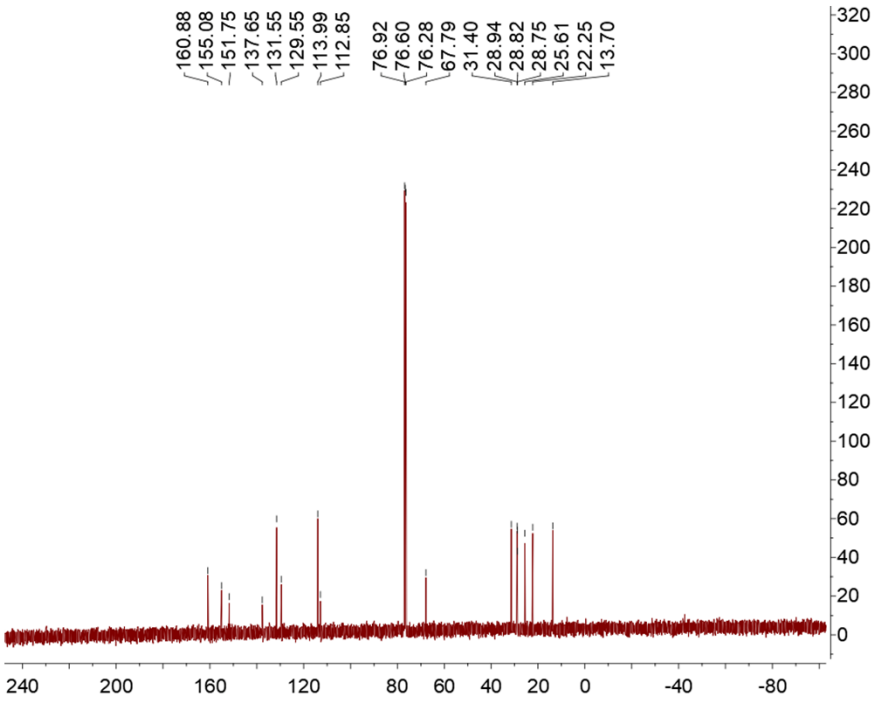

Supporting Figure S2. ^{13}C NMR of the monomer 1. $CDCl_3$ was used as the solvent.

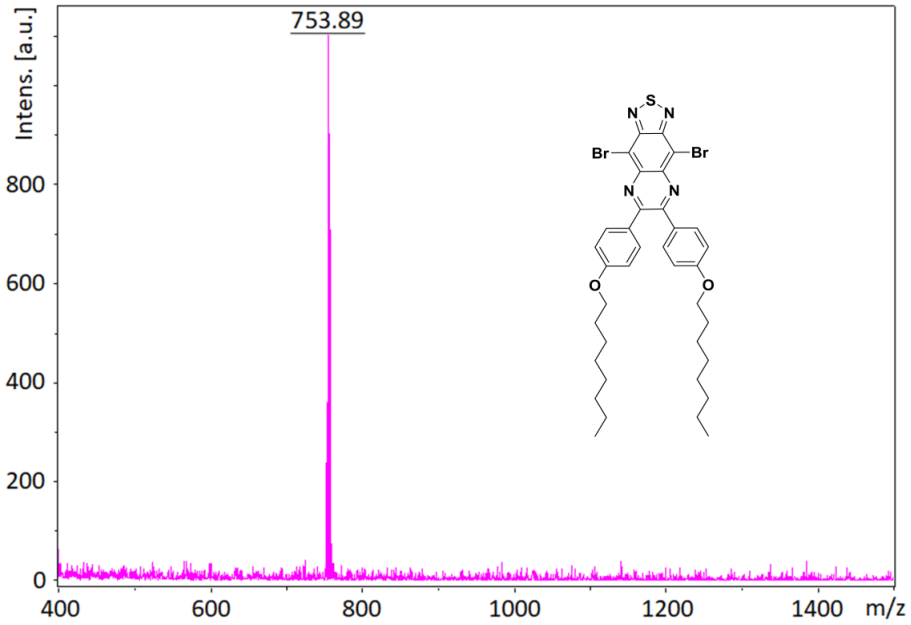

Supporting Figure S3. Matrix-assisted laser desorption/ionization time-of-flight (MALDI-TOF) mass spectrum of monomer 1 (M1).

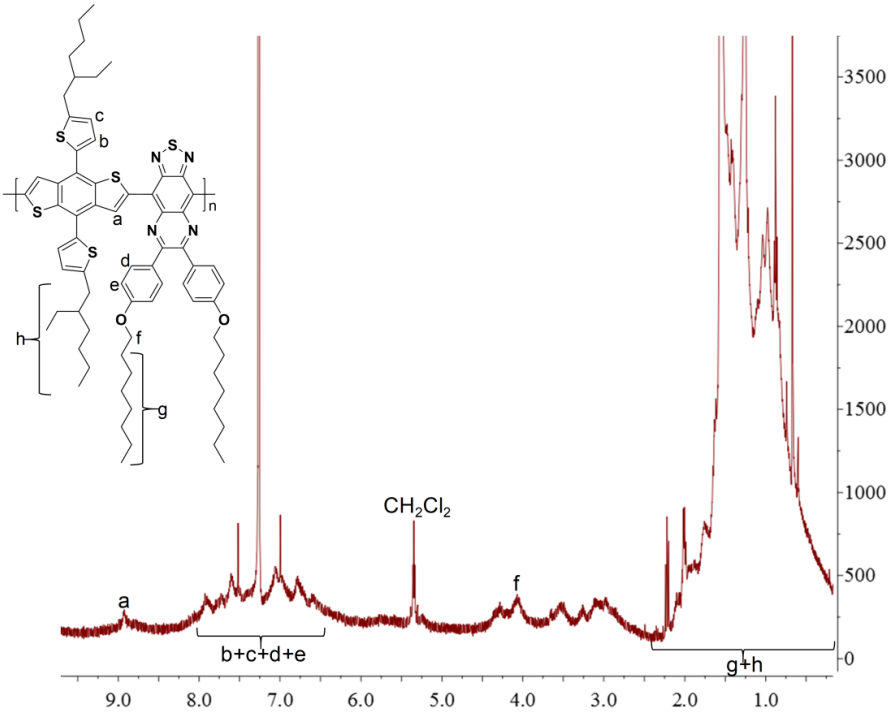

Supporting Figure S4. ^{1}H NMR of the semiconducting polymer (SP). $CDCl_3$ was used as the solvent.

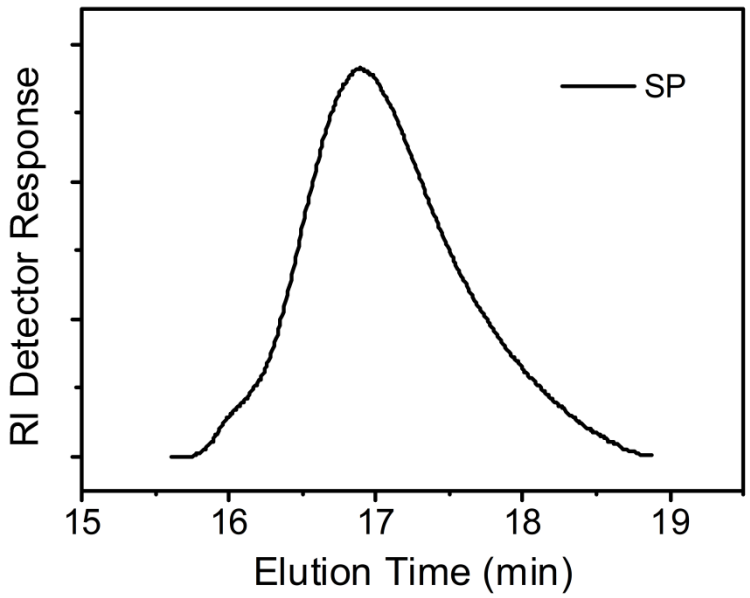

Supporting Figure S5. Gel permeation chromatogram (GPC) curve of the semiconducting polymer (SP).

Table S1. Gel permeation chromatogram (GPC) results of the SP.

Sample name	Mn	Mw	PDI
SP	39800	50100	1.26

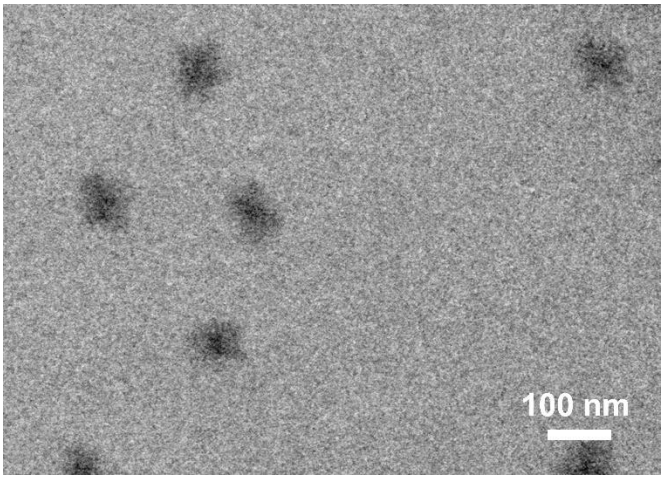

Supporting Figure S6. Representative transmission electron microscopy (TEM) image of the nanoparticles ($OSPNs^-$).

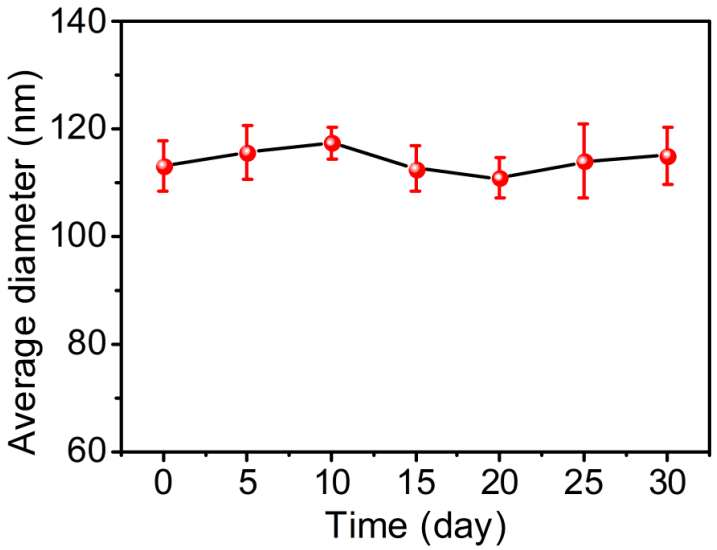

Supporting Figure S7. Average hydrodynamic diameters of the OSPNs^{+} stored in aqueous solution for different time periods (0-30 days).

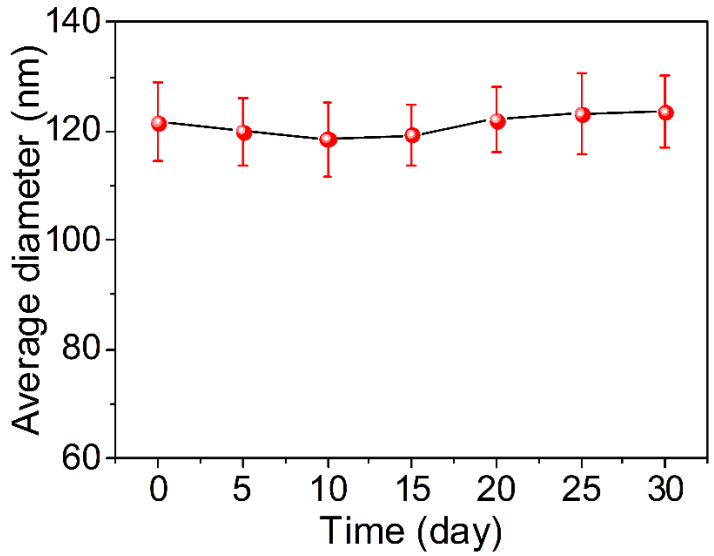

Supporting Figure S8. Average hydrodynamic diameters of the OSPNs^{+} stored in 10% fetal bovine serum (FBS) solution for different time periods (0-30 days).

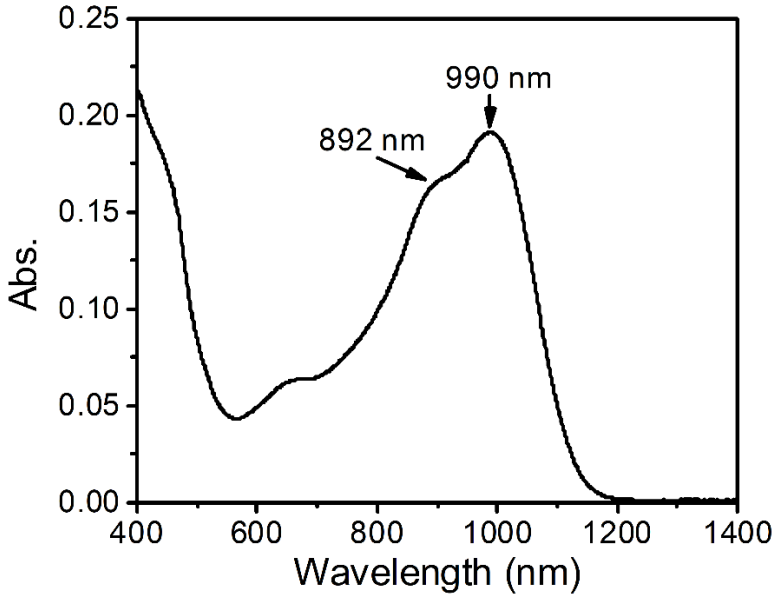

Supporting Figure S9. Absorption spectrum of the semiconducting polymer (SP) in tetrahydrofuran.

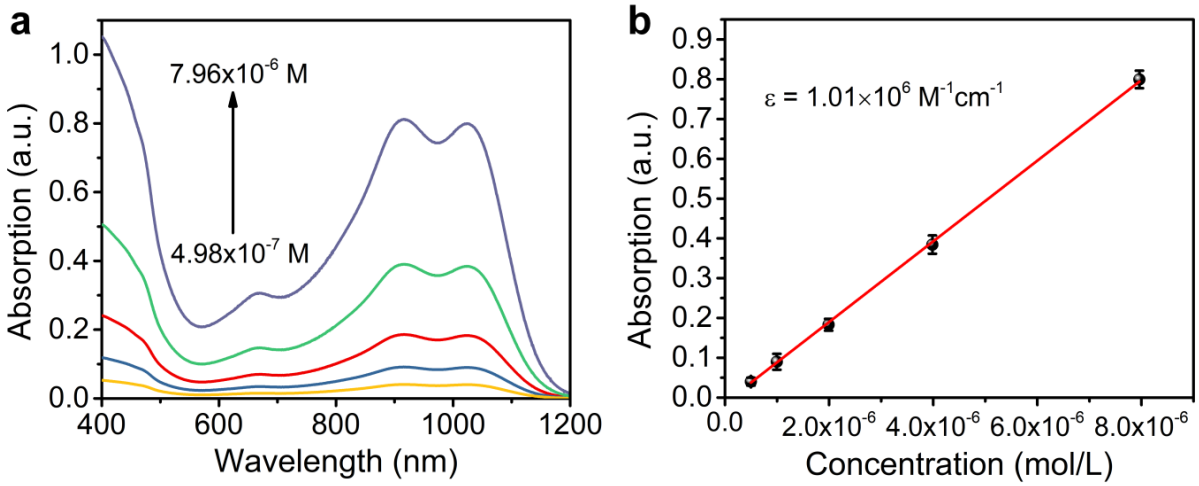

Supporting Figure S10. a) The absorption spectra of $OSPNs^+$ aqueous solution with different concentrations ranging from 4.98×10^{-7} M to 7.96×10^{-6} M. b) The plot of absorbance at 1025 nm versus $OSPNs^+$ concentrations. The red line represents linear fitting, which indicates the effective molar extinction capability of the $OSPNs^+$ with a molar absorption coefficient of 1.01×10^6 M^{-1} cm^{-1}. The error bars represent the standard deviation of three separate measurements.

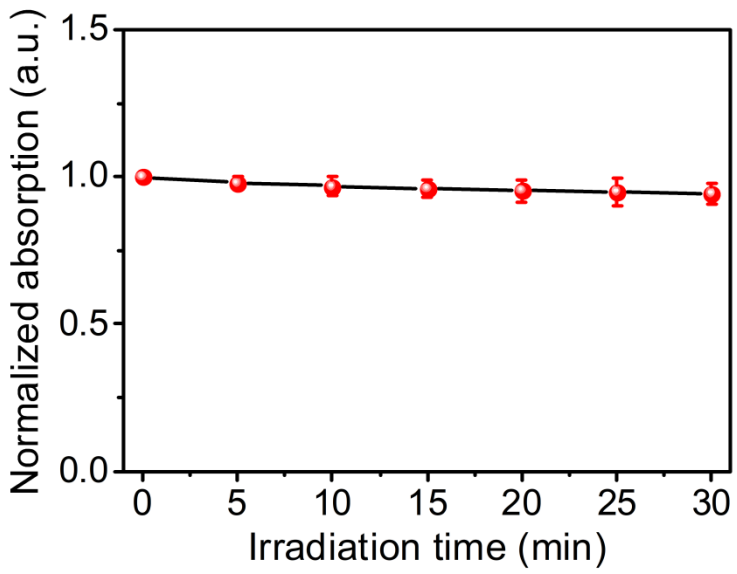

Supporting Figure S11. Normalized absorption fluctuation of $OSPNs^{+}$ at 1064 nm (Ab_{1064}) under 1064 nm laser excitation for 30 min. The laser energy density is fixed at 5.0 mJ/cm^2.

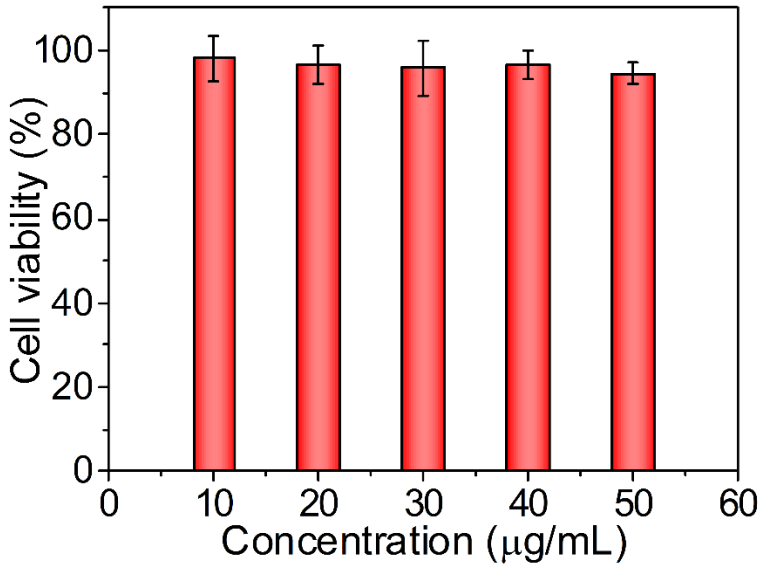

Supporting Figure S12. The methyl thiazolyl tetrazolium (MTT) assay of hMSCs treated by $OSPNs^{-}$ for 12 h under various concentrations.

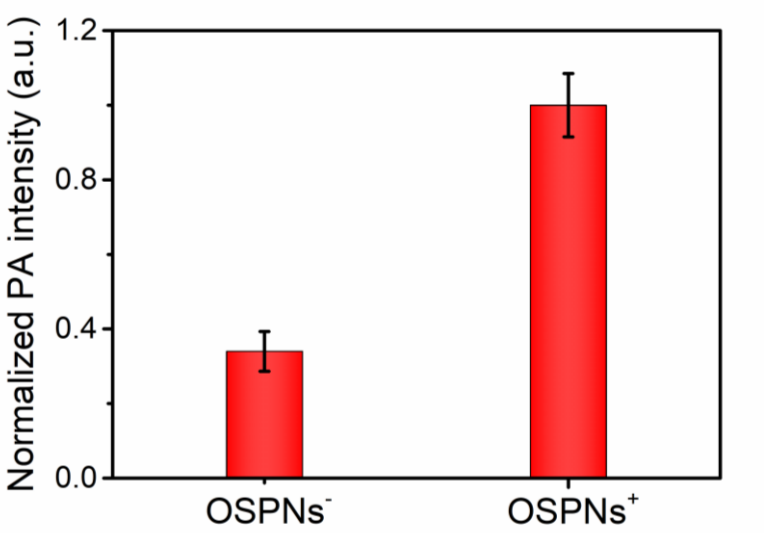

Supporting Figure S13. Comparison of the photoacoustic intensities of human mesenchymal stem cells (hMSCs) stained with $OSPNs^-$ and $OSPNs^+$. The error bars represent the standard deviation of three separate measurements.

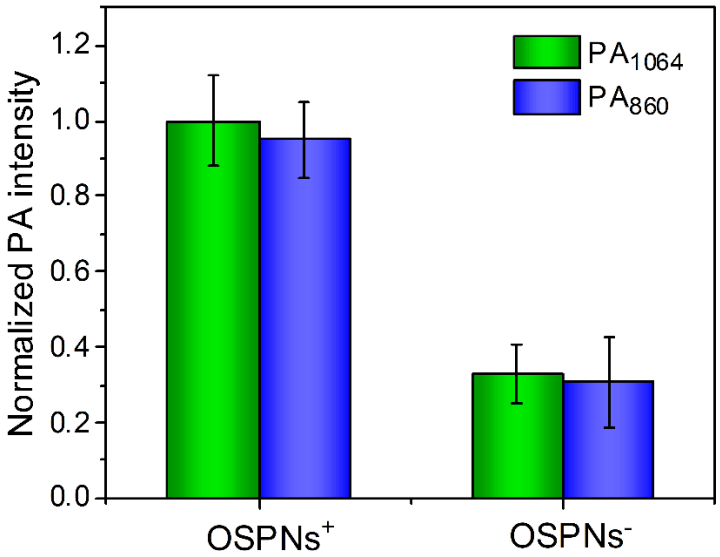

Supporting Figure S14. Quantitative analysis of PA intensities recorded at 860 and 1064 nm of $OSPNs^-$-and $OSPNs^+$-labelled cell pellets.

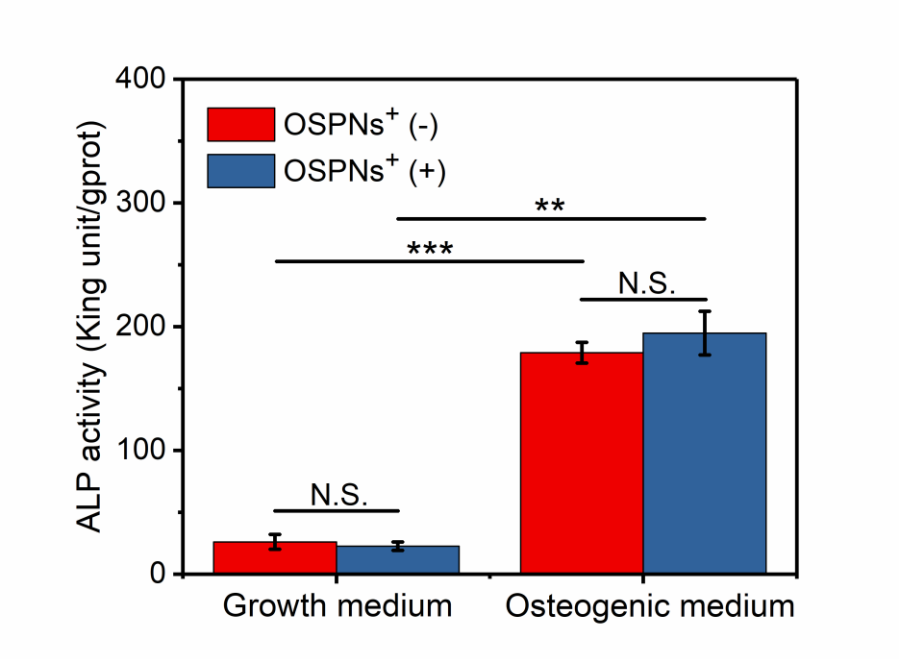

Supporting Figure S15. Alkaline phosphatase (ALP) activity detection of hMSCs incubated with growth medium or osteogenic medium for 14 days in the presence or absence of $OSPNs^+$ (**p < 0.01, ***p < 0.001, N.S.: no significant difference).

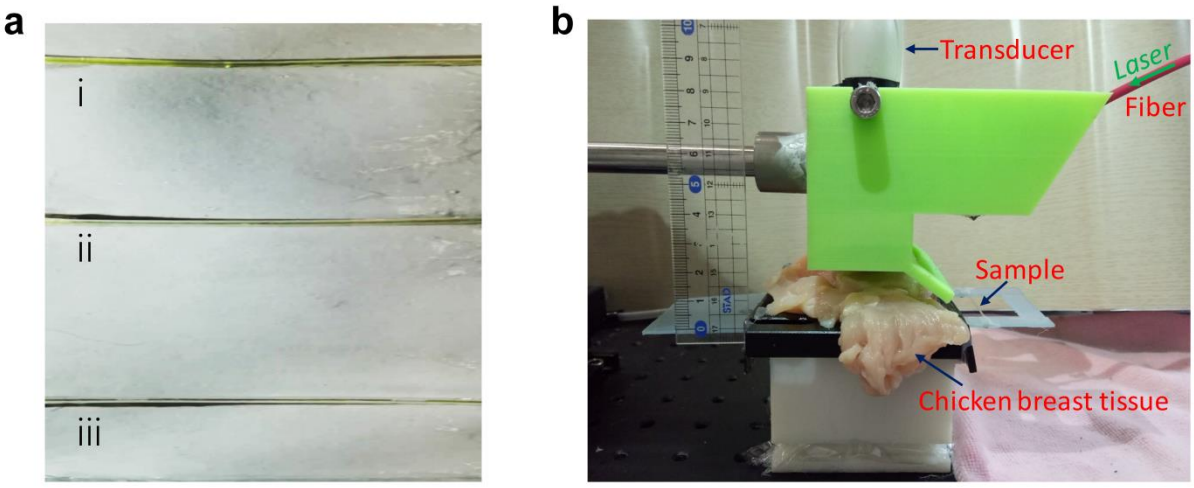

Supporting Figure S16. a) Photograph of $OSPNs^+$ aqueous solutions sealed into rubber tubes with various concentrations. i: 0.573 mg/mL; ii: 0.286 mg/mL; and iii: 0.143 mg/mL. b) Photograph of the chicken breast tissue model. The rubber tubes containing $OSPNs^+$ aqueous solutions were placed under the chicken breast tissue layers. The transducer was bound together with a fibre and tightly placed over the tissues.

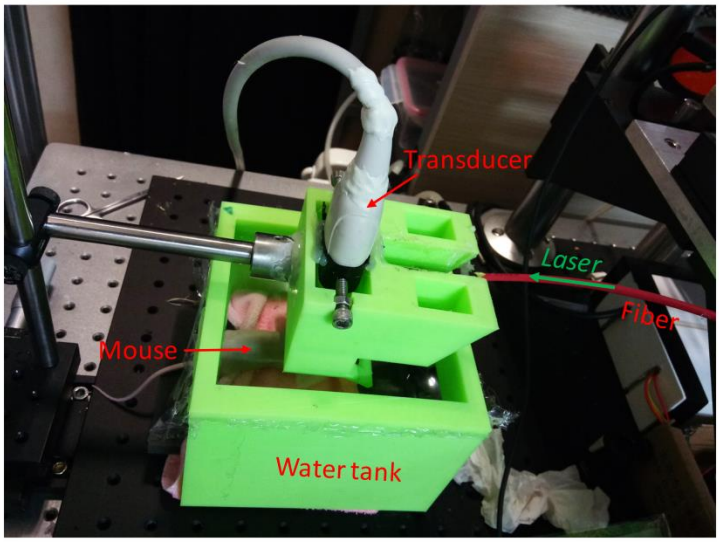

Supporting Figure S17. Photograph of the *in vivo* photoacoustic imaging using the photoacoustic computed tomography (PACT) instrument.

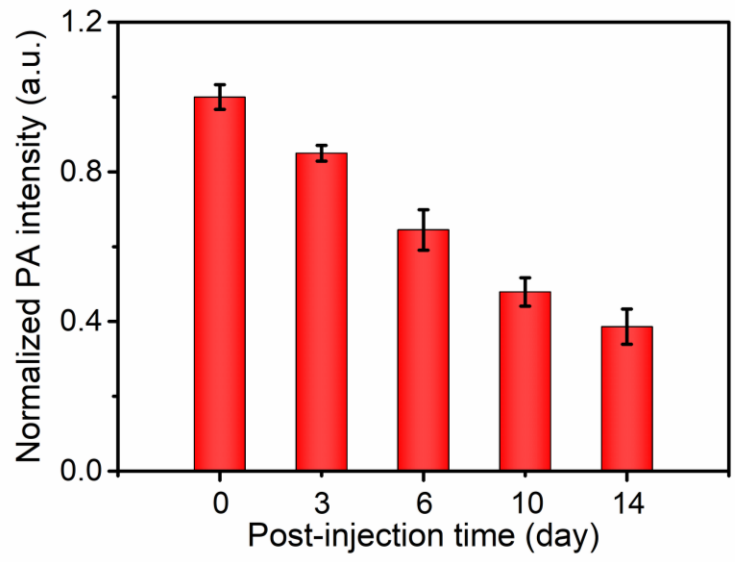

Supporting Figure S18. Photoacoustic signal quantification of OSPNs^{+}-labelled stem cells subcutaneously implanted into nude mice at different post-injection times.

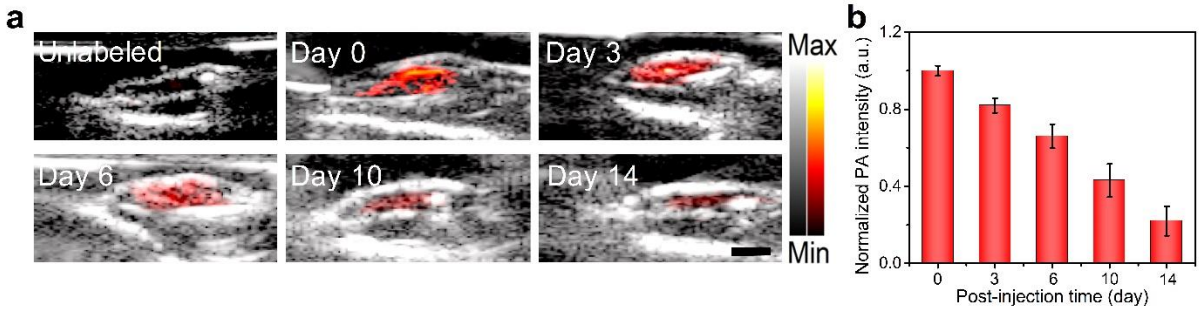

Supporting Figure S19. a) Merged ultrasound (US, grey scale) and PA (red-yellow scale) images of subcutaneously transplanted unlabelled or OSPNs$^-$-labelled hMSCs (10^5 cells). After incubation with or without OSPNs$^-$ (50 μg/mL) for 12 h, the cells were collected and mixed in 50% Matrigel/PBS (100 μL) followed by subcutaneous injection. Images of OSPNs$^-$-labelled cells were acquired serially at different post-injection time (day 0, 3, 6, 10, and 14). PA signals were recorded at 1064 nm with the energy density of 5 mJ/cm^2. Scale bar: 3 mm. b) PA signal quantification of OSPNs$^-$-labelled stem cells subcutaneously implanted into nude mice at different post-injection times.

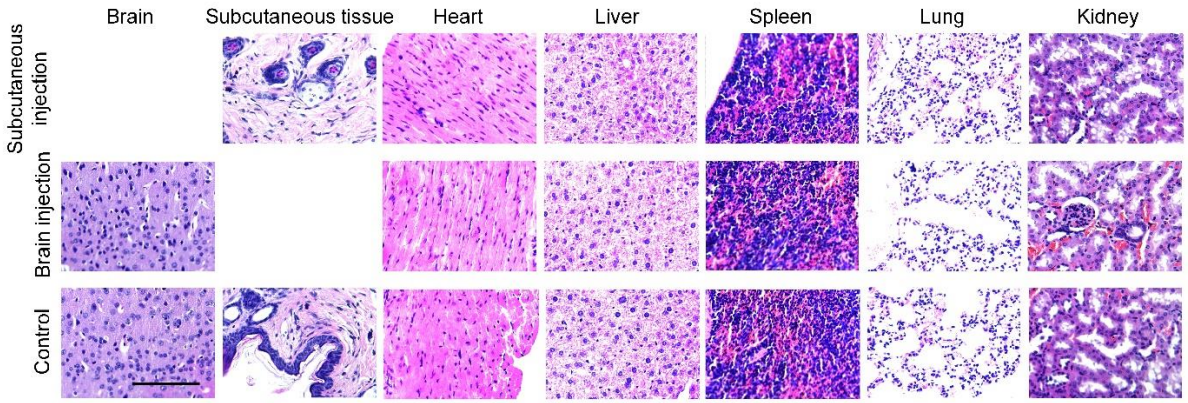

Supporting Figure S20. H&E staining of brain, subcutaneous tissues, and major organs from nude mice 14 days after receiving subcutaneous or intracranial injection of OSPNs$^+$-labelled stem cells. Scale bar: 100 μm.

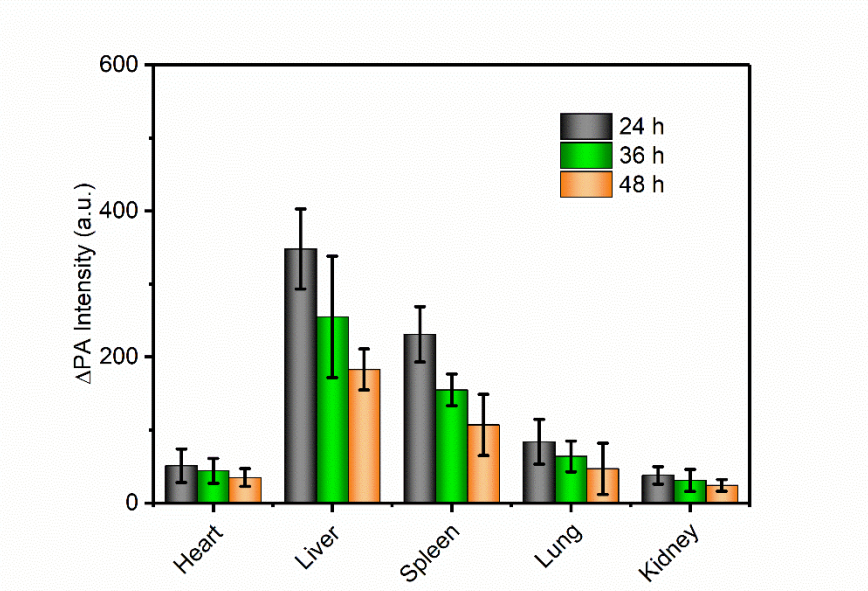

Supporting Figure S21. *Ex vivo* quantification of PA signals recorded at 1064 nm of major organs excised from nude mice 24, 36, and 48 h after tail vein injection of $OSPNs^{+}$ (120 μL, 0.1 mg/mL). Error bars represent standard deviations of three separate measurements.

2. Synthesis of Intermediates

*Synthesis of 4,7-Dibromo-5,6-dinitrobenzo[c][1,2,5]thiadiazole (**2**).*

In a 100-mL flask, 4,7-dibromobenzo[*c*][1,2,5]thiadiazole (1) (3 g, 10.2 mmol), sulfuric acid (12 mL), and nitric acid (70%, 12 mL) were mixed at 0℃. After stirring for 12 h at 100℃, the mixture was cooled to room temperature and poured into ice water. Then, NaOH was added into the solution. The precipitation was filtered, which was further purified by column chromatography to afford 2 as a white solid (959 mg, yield: 24.5%). ^{13}C NMR (DMSO-d_6, ppm) δ: 152.04, 144.22, 111.91. MS (m/z): 384.1 [M^+].

*Synthesis of 4,7-Dibromobenzo[c][1,2,5]thiadiazole-5,6-diamine (**3**).*

To a mixture of 2 (900 mg, 2.34 mmol) and iron powder (1.54 g, 27.6 mmol) was injected acetic acid (50 mL). After stirring at 80℃ for 6 h, the mixture was cooled to room temperature and filtered off. The filtrate containing 3 was collected for further use without purification.

*Synthesis of 1,2-Bis(4-hydroxyphenyl)ethane-1,2-dione (**5**).*

4,4'-Dimethoxy-benzil (4) (7.5 g, 27.7 mmol) and pyridine hydrochloride (19.2 g, 166.2 mmol) were mixed and heated to 220°C. When the solid mixture was completely melted, heating was maintained for another 1 h. When the temperature decreased to 80°C, pure water (30 mL) was added to produce a suspension, which was filtered at ~40°C. Ethyl acetate was used to dissolve the filter residue, and the solution was dried using anhydrous $MgSO_4$. Afterwards, the concentrated crude product was purified by column chromatography to yield pure 5 as a yellow solid (6.2 g, yield: 92.5%). ^{1}H NMR (CD_4O, ppm) δ: 7.82 (d, 4H), 6.91 (d, 4H). MS (m/z): 241.9 [M^+].

*Synthesis of 1,2-Bis(4-(octyloxy)phenyl)ethane-1,2-dione (**6**).*

5 (5.0 g, 20.6 mmol), anhydrous potassium carbonate (12.24 g, 0.092 mol), tetrabutyl ammonium bromide (0.37 g, 1.15 mmol), and acetone (120 mL) were added in a 250-mL round-bottom flask. 1-Bromooctane (8.7 g, 45.3 mmol) was then added into the mixture,

which was refluxed for 24 h under nitrogen protection. After removing the precipitate, the filtrate was concentrated and then purified by column chromatography to yield pure 6 (8.3 g, yield: 86.5%). ^{1}H NMR ($CDCl_3$, ppm) δ: 7.92 (d, 4H), 6.93 (d, 4H), 4.08 (t, 4H), 1.75 (m, 4H), 1.25-1.50 (m, 20H), 0.88 (t, 6H). MS (m/z): 466.1 [M^+].

*Synthesis of 4,9-Dibromo-6,7-bis(4-(octyloxy)phenyl)-[1,2,5]thiadiazolo[3,4-g]quinoxaline (**M1**).*

The previously resultant filtrate containing 3 was mixed with compound 6 (1.09 g, 2.34 mmol), and the mixture was stirred at 135°C for 1 day under N_2 protection. After solvent removal, the crude product was purified by column chromatography to afford pure M1 as an orange solid (0.85 g, yield: 48.2%). ^{1}H NMR ($CDCl_3$, ppm) δ: 7.75 (d, 4H), 6.92 (d, 4H), 4.02 (t, 4H), 1.81 (m, 4H), 1.47 (m, 4H), 1.24-1.39 (m, 16H), 0.89 (t, 6H). ^{13}C NMR ($CDCl_3$, ppm) δ: 160.88, 155.08, 151.75, 137.65, 131.55, 129.55, 113.99, 112.85, 67.79, 31.40, 28.94, 28.82, 28.75, 25.61, 22.25, 13.70. MALDI-TOF mass (m/z): 753.89 [M^+].